

Analysis and optimization of propagation losses in LiNbO₃ optical waveguides produced by swift heavy-ion irradiation

M. Jubera · J. Villarroel · A. García-Cabañes ·
M. Carrascosa · J. Olivares · E. Agullo-López ·
A. Méndez · J.B. Ramiro

Abstract The propagation losses (PL) of lithium niobate optical planar waveguides fabricated by swift heavy-ion irradiation (SHI), an alternative to conventional ion implantation, have been investigated and optimized. For waveguide fabrication, congruently melting LiNbO₃ substrates were irradiated with F ions at 20 MeV or 30 MeV and fluences in the range 10^{13} – 10^{14} cm⁻². The influence of the temperature and time of post-irradiation annealing treatments has been systematically studied. Optimum propagation losses lower than 0.5 dB/cm have been obtained for both TE and TM modes, after a two-stage annealing treatment at 350 and 375°C. Possible loss mechanisms are discussed.

1 Introduction

Recently, a method to produce optical waveguides on LiNbO₃ substrates by ion-beam irradiation [1–3] has been proposed and developed. At difference with conventional ion implantation that uses light ions (H, He) and relatively

low energies (1–3 MeV), the method involves irradiation with ions of high energy (tens of MeV) and moderate mass, such as F at 20 MeV, often designated as swift-heavy ions (SHI). In the SHI regime, the electronic stopping power S_e of the projectile ions is strongly dominant over the nuclear stopping for most of the trajectory excepting at the end of the ion range where implantation and nuclear damage take place. A key feature of the method is that the electronic stopping power of the bombarding ions surpasses a threshold value for material amorphization at a depth inside the crystal. Then a buried amorphous layer of isotropic low refractive index ($n = 2.10$) is generated at such depth by electronic processes instead of nuclear collisions. The typical layered structure, and the refractive index profile of the generated waveguide, is shown in Fig. 1. In Fig. 1a, it can be appreciated the crystalline guiding layer, followed by the amorphous barrier produced by electronic damage. The position of the implanted layer can be also seen at a deeper depth in the substrate although it does not play any role in waveguide operation. This is why we call these guides ion irradiated instead of ion implanted waveguides. Figure 1b, illustrates the typical index profile for the SHI waveguide structure (guiding layer and optical amorphous barrier) for both the ordinary and extraordinary refractive indexes.

The fabricated waveguides present several relevant advantages over those fabricated by conventional light ion implantation [4–6]. For example, they have step-like and high-jump index profiles (~ 0.2 and ~ 0.1 for ordinary and extraordinary refractive indexes, respectively, see Fig. 1b) and thick easily programmable amorphous layers which allow for supporting highly confined propagation modes. Moreover, low irradiation fluence is sufficient ($\approx 10^{14}$ cm⁻²) to produce the waveguides, so that the fabrication time may be reduced up to two orders of magnitude in comparison with the implantation case. Finally, good nonlinear optical

and photorefractive properties have been recently reported [3, 7, 8]. However, the preliminary reported values for PL yielded values ranging between 1–10 dB/cm [1, 8], which are still high for many applications, leaving much room for improvement and optimization.

The purpose of this work is to systematically address the topic of propagation losses (PL) for the SHI waveguides and look for an optimized response. Suitable post-irradiation annealing treatments were implemented in order to reduce absorption and scattering centers. Moreover, those treatments may improve the quality of the interface between the waveguiding and amorphous layers. However, one has to assure that the amorphous barrier is kept thick enough to avoid a substantial enhancement of the tunnelling losses. The relevance of this latter loss mechanism has been evaluated with the help of a beam propagation method (BPM). As a result of the study, we have demonstrated the feasibility of markedly reduced optical losses reaching values under 0.5 dB/cm for both TE and TM polarizations. This confirms that the novel

SHI waveguides are, indeed, very promising candidates for a variety of photonic devices.

2 Experimental techniques

Several waveguides have been fabricated by irradiation with fluorine ions at 20, and 30 MeV, on *z*-cut congruently melting lithium niobate substrates purchased from Photox in the 5 MV Tandem Accelerator of the CMAM at University Autónoma of Madrid [9]. In order to facilitate PL measurements, by using long waveguides (~ 2 cm length), substrate irradiation have been mostly performed under large incidence angles (70°). The energies, stopping powers, ion ranges, and fluencies used in this work are specified in Table 1. According with these irradiation parameters, the fabricated waveguides have been labelled or classified as type I, II, and III (see Table 1). The barrier thicknesses for the waveguides prior to annealing were estimated from the analysis reported in [3]. In order to investigate possible reduction of PL, after irradiation, samples have been subjected to annealing treatments, either isochronal (for 1 h) in the temperature range (250 – 375°C) or isothermal (at 300 and 350°C). Most of the annealing treatments were carried out in an oxygen atmosphere to avoid the generation of oxygen vacancy centers and reduction of impurity centers (e.g., Fe) [10]. However, no significant differences have been found with regard to thermal annealing in air.

The waveguides before and after annealing have been characterized by measuring the refractive index TE (ordinary refractive index n_o) and TM (extraordinary refractive index n_e) profiles using the prism-coupling *m*-line method with $\lambda = 632.8$ nm.

The PL were determined through the decay of the light intensity guided mode at $\lambda = 632.8$ nm, measured via the light scattered along the beam path [11] recorded by a CCD camera.

3 Waveguide losses: effect of annealing treatments

3.1 Role of temperature for isochronal annealing treatments

Successive one-hour-long annealing treatments at increasing temperatures separated 25°C inside the range 250 – 375°C

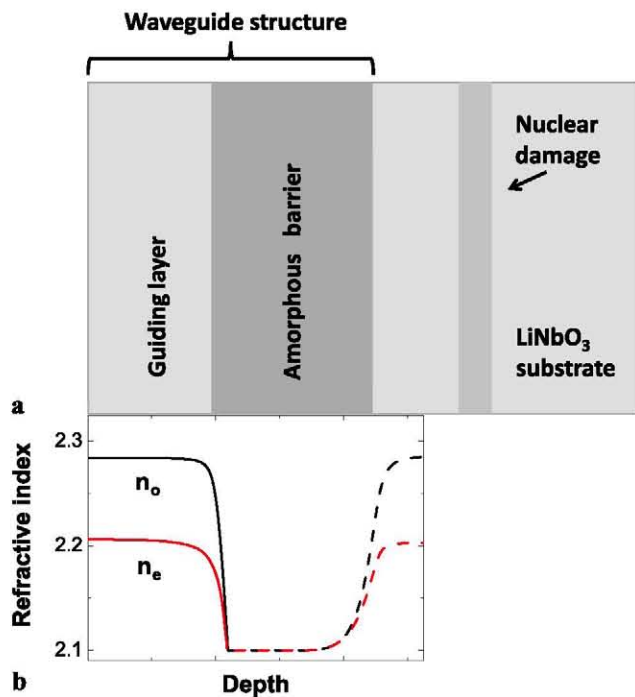


Fig. 1 (a) Schematics of the structure and (b) refractive index waveguide profile generated by swift-heavy ion irradiation of LiNbO₃ crystal

Table 1 Fabrication parameters and estimated barrier thickness [3] of the waveguides

Waveguide type	Ion, energy, incidence angle	Fluence (cm^{-2})	Barrier thickness h (μm)
Type I (guide A)	F, 30 MeV, 70°	2×10^{14}	0.8
Type II (guide B, C, D)	F, 30 MeV, 70°	3×10^{14}	0.9
Type III (guide E)	F, 20 MeV, 0°	4×10^{14}	3.0

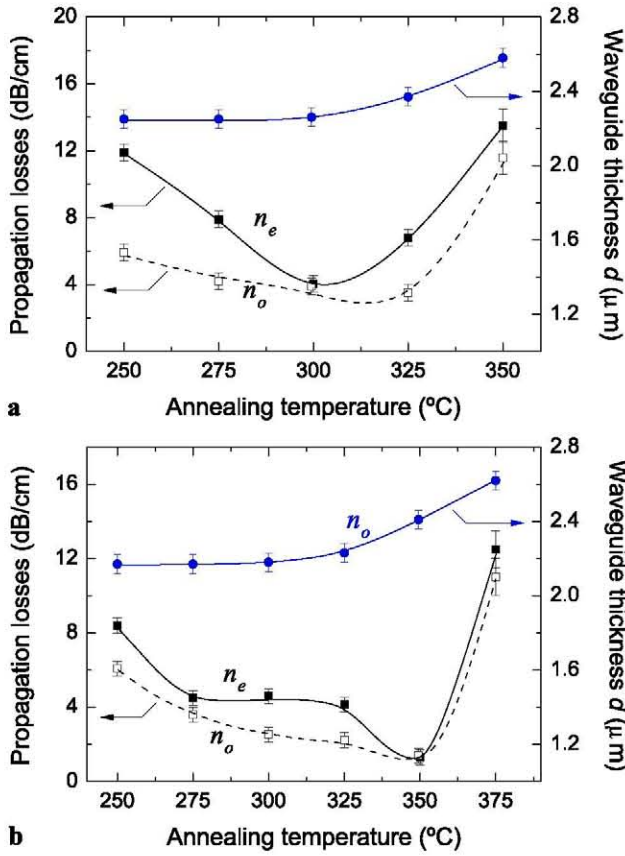


Fig. 2 Propagation losses and effective waveguide thickness vs. previous annealing temperature for (a) waveguide A and (b) waveguide B. *Continuous and dashed curves are only guides to the eye*

have been carried out. The measured PL for the fundamental mode are shown in Fig. 2 of guide A (Fig. 2a) and B (Fig. 2b), as a function of the temperature T of the annealing. The two polarizations ordinary (TE) and extraordinary (TM) are considered. The waveguide thickness d , obtained from the refractive index profiles measured after each treatment, is also included in the plot. The curves show a clear reduction in PL followed by a rapid enhancement for temperatures above 325 and 350°C for guides of type I and II, respectively. A minimum attenuation coefficient of about 1.2 dB/cm, is obtained for the TE (ordinary) polarization after the highest fluence of $3 \times 10^{14} \text{ cm}^{-2}$ and annealing at 350°C. Somewhat higher values are achieved for the guide fabricated at $2 \times 10^{14} \text{ cm}^{-2}$ ($>3 \text{ dB/cm}$). For TM (extraordinary) polarization, PL are generally higher, although a similar minimum value of 1.3 dB/cm is obtained at 350°C. It is significant that for both waveguides and both polarizations, the losses experience a dramatic enhancement when the annealing temperature rises above 325–350°C, coinciding with an appreciable increase of waveguide thickness.

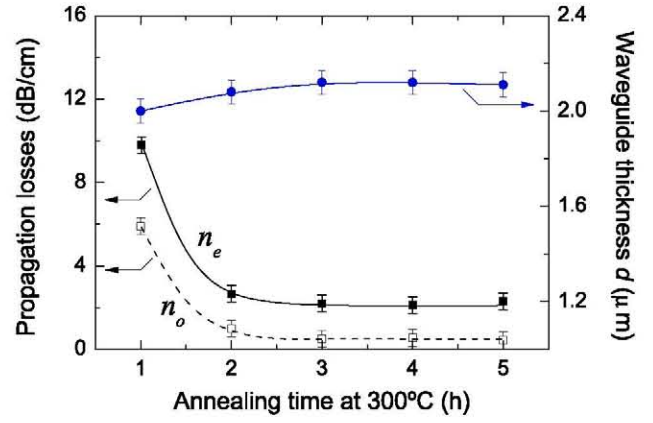


Fig. 3 Propagation losses and effective waveguide thickness vs. annealing time at 300°C for waveguide C of type II. *Continuous and dashed curves are only guides to the eye*

3.2 Role of time for isothermal annealing treatments

For a detailed investigation of the effect of annealing time, at a temperature close to the minima of losses in Fig. 2, isothermal treatments have been performed for guides of type II. In Fig. 3, the results for successive 1 h annealings at a constant temperature of 300°C and both polarizations TE and TM are shown. The evolution of the waveguide thickness after the various treatments is also plotted. Note that the treatments at constant temperature do not significantly affect the waveguide thickness. The PL initially decrease up to an essentially constant value, after 2–3 h. For TE modes, this value is well below 1 dB/cm; significantly lower than previously reported measurements for SHI waveguides [1, 8].

In order to investigate the possibility of a further reduction of PL, a higher temperature of 350°C was also checked for the same guide type II (guide D). Results are given in Fig. 4. The two polarizations TE (Fig. 4a) and TM (Fig. 4b) and the fundamental ($m = 0$) and the first-order ($m = 1$) modes have been measured. The optimum values for the fundamental mode are similar to those reached at 300°C for both polarizations. The first-order mode shows a decrease of propagation losses followed by an increase after about 3 h of annealing.

4 Discussion

The above results show that the evolution of the PL with annealing temperature for the novel SHI waveguides presents two different regions. In the initial stage, increasing temperature up to around 300 or 350°C (depending on the waveguide type) causes a clear reduction in waveguide losses. This stage is very likely related to the removal of radiation induced coloring and defects centers, in accordance with results reported in the literature for waveguides prepared by different ion implantation processes [4, 12–17].

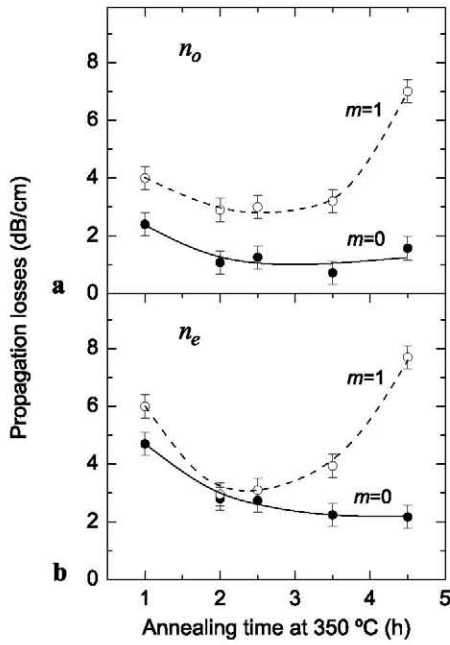


Fig. 4 Propagation losses of the fundamental ($m = 0$) and first order ($m = 1$) mode vs. annealing time at 350°C for waveguide D (a) ordinary, (b) extraordinary polarization. *Continuous* and *dashed* curves are only guides to the eye

Another source of PL is the scattering at the interface separating the guiding and barrier layers. For our waveguides, it is expected that the interface has some roughness due to the statistical fluctuations caused by the overlapping of the amorphous tracks associated to individual ion trajectories [18]. Since the statistical roughness should decrease with increasing irradiation fluence, one would predict that losses decrease with fluence, in accordance with the observed data. In a second stage at higher temperatures, there is a competing effect due to the narrowing of the optical barrier. The rapid increase of PL observed in Figs. 2a and 2b at higher temperatures suggests an enhanced tunnelling effect. In line with this idea, this fast enhancement of losses is not observed in the isothermal experiment at 300°C (Fig. 3), where the barrier thickness keeps essentially constant. On the other hand, the isothermal experiment at 350°C (Fig. 4) shows a similar saturating behaviour of PL for the fundamental mode; whereas the first mode, more sensitive to the tunnelling through the barrier, exhibits a strong increase in PL for $t > 2.30$ h. Therefore, it may be concluded that in previous experiments, the tunnelling mechanism is responsible for the saturation behaviour appearing in the explored route to reduce losses.

A further confirmation of the tunnelling mechanism being responsible for the rise in losses in the second stage ($T > 300$ – 350 °C), is obtained from calculations using the beam propagation method (BPM) to describe light propagation through the waveguiding structure. The simulations have been performed using the 2-dimension Crank–Nicolson fi-

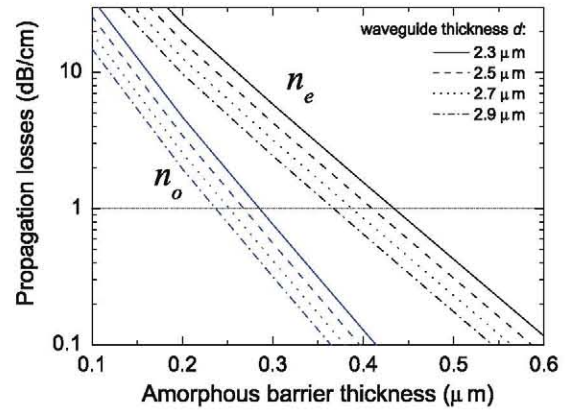


Fig. 5 Tunnelling losses as a function of the barrier thickness for several waveguide widths and ordinary and extraordinary polarizations calculated using a BPM

nite differences scheme for beam propagation method [19]. This method considers the waveguide as a set of very thin strips perpendicular to the propagation direction. Prior to the simulation, the guided modes of the waveguide are computed and the selected one is introduced into the waveguide. This initial condition is used to determine the electric field for each cell of the following strip. Calculations show the light intensity of the guided wave decreasing along the propagation direction due to the tunnelling losses. This BPM method has been already used to discuss photorefractive phenomena in LiNbO₃ waveguides [20].

Figure 5 shows the predicted tunnelling losses as a function of the barrier thickness for several waveguide thicknesses just in the range of our experimental values (see Figs. 2 and 3). Tunnelling losses rapidly (exponentially) increase with the reduction of barrier thickness so that they overpass 1 dB/cm for barrier thickness lower than 0.25–0.3 μm and 0.4–0.45 μm for ordinary and extraordinary polarization, respectively. In order to compare our experimental data with these theoretical predictions, it is necessary to estimate the barrier thickness of our guides after each annealing step. Note that annealing treatments reduce the amorphous barrier thickness h by epitaxial recrystallization [21], whereas they increase in the same amount the waveguide thickness d . Then, for our estimates, we subtract from the initial barrier thickness h (see Table 1) the amount $2\Delta d$, assuming that both barrier boundaries recrystallize at the same speed. In fact, the estimated barrier evolution is roughly consistent with the thermally activated crystallization velocity reported in [21]. In Fig. 6, the estimated values of the waveguide barrier h are plotted together with the measured propagation losses and the predicted tunnelling losses for the experiment of Fig. 2a for TM polarization. It can be clearly appreciated that predicted tunnelling losses are negligible throughout the first stage of the curve but rapidly increase for $T > 325$ °C, coinciding with the sudden increase

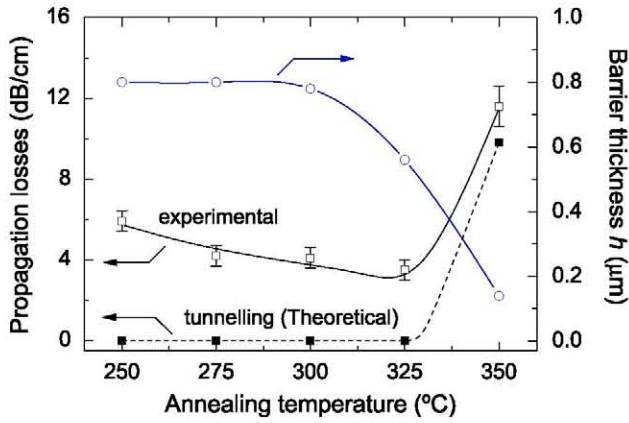


Fig. 6 Estimated values of the waveguide barrier thickness h (circles) experimental propagation losses taken from Fig. 2a (empty squares) and predicted tunnelling losses (solid squares) vs. previous annealing temperature for waveguide A and TE mode propagation (see text). Continuous and dashed curves are only guides to the eye

of experimental PL. A similar behavior has been obtained for the waveguide B and for both polarizations; thus confirming that tunnelling losses are responsible for the rapid increase of PL in the second stage of the PL curves of Fig. 2.

In summary, the analysis performed so far suggests that further optimization of PL might be obtained by an additional rise of the annealing temperature, but avoiding the larger tunnelling losses associated with a reduced barrier thicknesses. This is what has been attempted in the next section.

5 Optimized waveguide

The previous discussion indicates that in the strategy to reduce PL, a key point is to fabricate waveguides with thicker optical barriers. To that end, we have fabricated a waveguide with fluorine irradiation at 20 MeV, a higher fluence of $4 \times 10^{14} \text{ cm}^{-2}$, and normal ion incidence (guide E, type III). In this case, the optical amorphous barrier is about $3 \mu\text{m}$ [3].

The experimental procedure implies a two stage annealing treatment. First, we performed 1 h annealing at 350°C and next, a final 15 min annealing at 375°C . PL were measured after each partial treatment. The results are summarized in Table 2. As expected, the annealing at 350°C , leads to an important reduction of PL, up to a value similar to those measured for the waveguides of type II. However, a definite improvement was achieved after the final short treatment at 375°C at which the optical barrier still keeps a sufficient thickness to limit tunnelling losses. The final outcome of this experiment is that PL reach optimum values of $\leq 0.5 \text{ dB/cm}$ for both polarizations. For the ordinary polarization, losses are even below 0.3 dB/cm . These values are, comparable or even better than those measured for

Table 2 Values of propagation losses (PL) and waveguide thickness d , measured in the waveguide of type III after the annealing treatments, which are also indicated in the table. n_o and n_e indicate ordinary and extraordinary polarizations, respectively

T ($^\circ\text{C}$)	Time (h)	PL - n_o (dB/cm)	PL - n_e (dB/cm)	d (μm)
350	1	0.3	1.5	2.8
375	0.25	<0.3	0.5	3.0

any other type of LiNbO₃ waveguides, including those fabricated either by standard implantation [22, 23] or irradiation with high energy heavy ions [1, 8].

It is worthwhile remarking that the PL optimization method proposed in this work relies on two properties of swift-heavy ion irradiated waveguides: (i) the possibility to easily obtain thick amorphous barriers. Note that this is complicated for standard light ion implantation techniques that require multi-energy ion-implantation [23, 24] to enlarge the amorphous barrier and even in that case typical amorphous barriers are about 1 micrometer [24], (ii) the possibility to modify the barrier thickness by re-crystallization. This is accompanied by a simultaneous reduction of propagation losses for appropriate treatments.

6 Summary and conclusions

A systematic study of the reduction of PL for SHI waveguides through suitable post-irradiation annealing treatments has been carried out. As a result, we have demonstrated the feasibility of markedly reducing PL to values under 0.5 dB/cm for both polarizations.

We can then conclude that waveguide fabrication by swift-heavy ion irradiation has relevant advantages regarding to the conventional implantation method; not only when step-like high-jump index profiles are concerned but also concerning the control and optimization of propagation losses.

Acknowledgements This work has been supported by Ministerio de Ciencia e Innovación (MICINN) under grant MAT2008-06794-C03. M. Juberá acknowledges his FPI fellowship from MICINN.

References

1. J. Olivares, G. García, A. García-Navarro, F. Agulló-López, O. Caballero, A. García-Cabañes, *Appl. Phys. Lett.* **86**, 183501 (2005)
2. J. Olivares, A. Gracia-Navarro, A. Méndez, F. Agulló-López, G. García, A. García-Cabañes, M. Carrascosa, *Nucl. Instrum. Methods Phys. Res. B* **257**, 765 (2007)
3. J. Olivares, A. García-Navarro, G. García, F. Agulló-López, F. Agulló-Rueda, A. García-Cabañes, M. Carrascosa, *J. Appl. Phys.* **101**, 033512 (2007)
4. P.D. Townsend, P.J. Chandler, L. Zhang, *Optical Effects of Ion Implantation* (Cambridge University Press, Cambridge, 1994)

5. F. Cheng, X.-L. Wang, K.-M. Wang, *Opt. Mater.* **29**, 1523 (2007)
6. F. Cheng, *J. Appl. Phys.* **106**, 081101 (2009)
7. J. Villarroel, M. Carrascosa, A. García-Cabañes, O. Caballero-Calero, M. Crespillo, J. Olivares, *Appl. Phys. B* **95**, 429 (2009)
8. A. Majkic, M. Koechlin, G. Poberaj, P. Günter, *Opt. Express* **16**, 8769 (2008)
9. <http://www.cmam.uam.es>
10. A. García-Cabañes, E. Diéguez, J.M. Cabrera, F. Agulló-López, *J. Phys., Condens. Matter* **1**, 6453 (1989)
11. Y. Okamura, S. Yoshinaka, S. Yamamoto, *Appl. Opt.* **22**, 3892 (1983)
12. G. Gotz, H. Karge, *Nucl. Instrum. Methods Phys. Res. B* **209/210**, 1079 (1983)
13. A. Boudrioua, J.C. Loulergue, F. Laurell, P. Moretti, *J. Opt. Soc. Am.* **18**, 1832 (2001)
14. G.G. Bentini, M. Bianconi, M. Chiarini, L. Corra, C. Sada, P. Mazzoldi, N. Argiolas, M. Bazzan, R. Guzzi, *J. Appl. Phys.* **92**, 6477 (2002)
15. G.G. Bentini, M. Bianconi, L. Corra, M. Chiarini, P. Mazzoldi, C. Sada, N. Argiolas, M. Bazzan, R. Guzzi, *J. Appl. Phys.* **96**, 242 (2004)
16. K. Peithmann, M.R. Zamani-Meymian, M. Haaks, K. Maier, B. Andreas, K. Buse, H. Modrow, *Appl. Phys. B* **82**, 419 (2006)
17. K. Peithmann, P.D. Eversheim, J. Goetze, M. Haaks, H. Hattermann, S. Haubrich, F. Hinterberger, L. Jentjens, W. Mader, N.L. Raeth, H. Schmid, M.R. Zamani-Meymian, K. Maier, *Appl. Phys. B* **105**, 113 (2011)
18. A. Rivera, M.L. Crespillo, J. Olivares, G. García, F. Agulló-López, *Nucl. Instrum. Methods Phys. Res. B* **268**, 2249 (2010)
19. J. Ramiro-Díaz, A. Alcazar de Velasco, *IEEE Trans. Ultrason. Ferroelectr. Freq. Control* **380**, 71 (2009)
20. J. Villarroel, J. Carnicero, F. Luedtke, M. Carrascosa, A. García-Cabañes, J.M. Cabrera, A. Alcazar, B. Ramiro, *Opt. Express* **18**, 20852 (2010)
21. M.L. Crespillo, O. Caballero-Calero, V. Joco, A. Ribera, P. Herero, J. Olivares, F. Agulló-López, *Appl. Phys. A* **104**, 1143 (2011)
22. B. Vincent, A. Boudrioua, R. Kremer, P. Moretti, *Opt. Commun.* **247**, 461 (2005)
23. B. Vincent, R. Kremer, A. Boudrioua, P. Moretti, Y.C. Zhang, C.C. Hsu, L.H. Peng, *Appl. Phys. B* **89**, 235 (2007)
24. A. Dazzi, P. Mathey, P. Lompré, P. Jullien, *Opt. Commun.* **149**, 135 (1998)